Cement and Concrete Composites 73 (2016) 174–184

Contents lists available at ScienceDirect

Cement and Concrete Composites

journal homepage: www.elsevier.com/locate/cemconcomp

Reinforced and hardened three-phase-foams

Christina Krämer*, Onyi Merry Azubike, Reinhard H.F. Trettin

Universität Siegen, Institut für Bau- und Werkstoffchemie, Paul-Bonatz-Str. 9-11, Siegen, Germany

ARTICLE INFO

Article history:
Received 21 December 2015
Received in revised form
28 May 2016
Accepted 21 July 2016
Available online 25 July 2016

Keywords:
Nanoparticles
Inorganic foams
Three-phase-foams
Carbon nanotubes
Titanate nanotubes
Pozzolanic reaction

ABSTRACT

Currently and in the past several lightweight materials were evolved focusing on different applications. Many developments are based on biomimetic approaches to reach material and cost savings with a simultaneous combination of thermal insulation and sustainability, for example. The desire of needed high porosity and lower density lead to less strength of the materials. Thus, applications are limited. One way to solve this problem is the creation of foams based on three phases. A new approach is the implementation of nanotubes and further chemical treatment of the inorganic foams to avoid further energy consuming thermal treatment for strengthening. Three-phase-foams consist of pozzolanic active nanomaterials as a third phase, which can be varied and surface treated. The resulting materials can be combined with other binders to further improve their properties or used as self-contained materials.

Aided by chemical treatment a hardening of the foams has been achieved. Implementation of prefabricated and synthesized nanotubes as a nanoreinforcement were successfully done and properties of the foams investigated. Results based on studies of the microstructure and phase formation will be illustrated and discussed.

1. Introduction

1.1. State of knowledge

Nowadays, in food, cosmetic or construction industries foams are commonly used for further implementation or as self-contained materials [1,2]. Hereby, biomimetic approaches enable to develop new materials [3]. Following the definition of Bikerman in 1973 foams are colloidal systems and based on aggregation of two-phases. Commonly, foams are classified as gases dispersed in liquids but also gases dispersed in solids known as solid foams [4]. The former are wet foams and normally used for implementation in other binders to observe certain porosity [1]. Foams are unstable due to high surface energy resulting from the gas-liquid (disperse-continuous) interface. Caused by the large total area, interfacial properties like surface tension and elasticity influencing foam stability [5,6]. Surface tension is defined as the ratio of work required to increase the interface and the related change of interfacial area. For lowering the surface tension and free energy of the system, surfactants are used which adsorb at the gas-liquid interface. Surface tension decreases with increasing surfactant concentration until critical micelle concentration is reached. At this point surface tension is no longer reduced and with further increase more and more micelles are formed. Nevertheless, the metastable foam system collapses after a certain time through its effort to lower surface energy. Destabilizing effects like drainage, coalescence and Ostwald-ripening result in complete separation of disperse and continuous phase [6–10]. Furthermore, also colloidal particles can be introduced in the disperse-continuous interface which is dependent on the wetting property of the particle surface [11–16]. Pickering emulsion is hereby one of the oldest and well-known approaches of foam stabilization through particles which can be wetted by both disperse and continuous phase [11]. These partially hydrophobized particles are also observed by adsorption of surfactant molecules at solid-liquid-interfaces. Surface properties as surface tension and contact angle were determined through chemical composition of the three phases and temperature. Adsorption mechanisms are related to both the interaction between surfactant and particle and between surfactant molecules among themselves [12,17]. Several approaches of using long-chain surfactants or hydrophobic silanes were described to change particle surface properties. *Gonzenbach* et al. were the first group which showed high-volume particle stabilized foams which prevent drainage and fewer further destabilizing effects [18]. Due to the high content of modified particles in the liquid medium, high amounts of disperse-continuous interfacial area are stabilized.

* Corresponding author.
E-mail address: kraemer@chemie.uni-siegen.de (C. Krämer).

http://dx.doi.org/10.1016/j.cemconcomp.2016.07.012
0958-9465/

Thus, integration of particles in the gas-liquid (disperse-continuous) interface is enabled by electrostatic forces between the particles and surface-active agents which lead to a sorption on the particle surface. Resulting partially hydrophobized particles can also dip into the disperse phase and lead to high stability, along with a low density, even after complete water diffusion or drying of the foams [18–20].

1.2. Carbon and titanate nanotubes

In this study different nanotubes were used to improve foam performance and add their desired properties. First nanotubes synthesized were carbon nanotubes (CNTs) in 1951 by Radushkevich et al. [21]. Since Iijima et al. who published further investigations on their properties, nanotubes became an even greater focus of attention [22].

CNTs have good thermal conductivity of theoretically 6000 W/mK at room temperature. Measurements show 3500 W/mK in axial directions which is the ninefold value of copper [23]. Also, high thermal stability up to 750°C in air and 2800°C in vacuum, good electrical conductivity, low density of 1.33–1.40 g/cm^3 including the cavity volume and tensile strength of 11–150 GPa are advantageous properties of CNTs [24–26]. The structure of CNTs is equal to coiled graphite layers. Thus, carbon is sp^2 hybridized in an aromatic ring structure and can be single-walled or multi-walled. Single-walled CNTs have diameters of 1–2 nm and three types of nanotubes are distinguished: armchair, zigzag, and chiral which have an influence on the electrical properties. There are mainly three different ways used to synthesize CNTs: arc-discharge method, laser ablation technique and chemical vapor deposition (CVD). Used prefabricated CNTs were produced by catalytic chemical vapor deposition (CCVD) a variation of CVD [22,27,28]. Due to the oxidation processes functionalities like carboxyl, carbonyl and hydroxyl groups are formed which are depending on the process and oxidant strength. Further on, CNTs can be coated by SiO_2 to improve the interaction with and thus implementation in other materials. Coating of CNTs is done in layers by adsorption of organic silicic acid ester like tetraethyl orthosilicate (TEOS) in addition with thermal decomposition or sol-gel method. SiO_2 layer thickness varies between 1 nm to several nanometers [29–33].

Compared to CNTs, titanate nanotubes (TiNTs) show differences in their structure and properties. TiNTs have a hydrophilic surface without any further treatment and consist in every case of several layers which are based on one coiled plane. Depending on the used synthesis and resulting structure different inner and outer diameters around 5.3 nm or 9.0 nm and 0.75–0.92 nm for the distance of the layers were published [34,35]. High resistance to alkaline conditions is one of the advantageous property. The stability to acidic environments is limited due to the conversion to rutile nanoparticles in strong acids [36]. In addition, TiNTs enable good ion exchange capability. Relating to the structural properties different descriptions can be found in the literature. Researchers found that the structure is similar to anatase [37–39] but also composition of TiO_x similar to rutile or anatase [34]. Also, structures related to sodium titanate or trititanic acid and their hydrated forms were postulated [35,40–44]. Nowadays, three different ways to synthesize TiNTs are used: template synthesis, anodic process and hydrothermal synthesis [45,46]. In our study, modified hydrothermal synthesis is used. Herefore, anatase is thermally treated in alkaline solution [37,47].

1.3. Hardening and nanoreinforcement

Following the approach of *Gonzenbach* et al. investigations on foams based on nanosilica (NS) as a third phase were done. Due to this, the resulting three-phase-foams can also be hardened by chemical treatment for certain applications to avoid energy consuming thermal treatment. After storage in $Ca(OH)_2$ solution, pozzolanic reaction of nanosilica particles to form strength improving calcium-silcate-hydrates (C-S-H), reach denser microstructure or packing in the borders/lamellae and healing of shrinkage cracks is enabled [20,48].

In our study, we show an approach to implement different nanotubes in the microstructure of three-phase-foams. This nanoreinforcement is combined with the hardening process in solution to further stabilize the foam structure and improve foam performance. Thus, three-phase-foams consist not only of an additional third solid phase of pozzolanic active nanoparticles but also nanotubes which can influence pozzolanic activity. This research is a continuation of foregone investigations on the improvement of foam performance in Refs. [20,49,50]. Nanotubes used are oxidized/SiO_2-coated carbon nanotubes and titanate nanotubes which are synthesized. Beside the goal to successfully implement these nanotubes in the foam structure, differences in the influence of nanotubes on microstructural properties, phase development and especially pozzolanic reactivity related to the surfactant should be elucidated. Thus, our experimental results enable the understanding and knowledge for further adaption as well as improvement of inorganic foams.

It is of importance for building and material chemistry because of the opportunity to reduce the content of inorganic binders. The research we present enables research scientists to produce stable inorganic foams with low densities of 60–90 kg/m^3 and a method for production of lightweight materials which are low cost energy saving materials due to material reduction. Also, the implemented nanotubes could provide additional electrical, thermal and photocatalytic properties to the foams. Moreover, these foams can also be used for foam concrete production and lead to enhanced materials properties as shown in Refs. [1,50,53,54].

2. Experimental section

2.1. Materials

2.1.1. Nanomaterials

The nanoparticles used were AEROSIL® 90 (Evonik). Prefabricated multi-walled CNTs (Bayer) were chemically treated to enhance the amount of functional groups like –COOH and –OH. Through a sol-gel process these oxidized CNTs (oxCNTs) were coated with SiO_2 (coatCNTs) and current TiNTs produced by modified hydrothermal synthesis (See 2.2 Specimen preparation).

The outer diameter of the used nanomaterials was measured by scanning electron microscopy (SEM) and with the help of gas adsorption the BET-surface (following **B**runauer-**E**mmert-**T**eller) was determined. A negative zeta potential was measured at pH 7 to 12 for all nanomaterials by electrophoretic light scattering. Zeta potentials are given at pH 10 which is the pH value of the dispersions used for foam preparation (Table 1).

2.1.2. Surface active agents

As surfactant TEGO Betain F 50 (Evonik) was used. According to

Table 1
Properties of the different nanomaterials.

	NS	oxCNTs	coatCNTs	TiNTs
BET-surface (m^2/g)	104 ± 10	219 ± 1	44 ± 1	149 ± 1
Diameter$_{outer}$ (nm)	~20	~10–20	~100–150	~10–30
Zetapotential$_{pH\ 10}$ (mV)	–48	–39	–50	–34

International Union of Pure and Applied Chemistry (IUPAC) cocamidopropyl betaine is also known as *N*-(carboxymethyl)-*N*,*N*-dimethyl-3-[(1-oxododecyl)amino]-1-propanaminium. The detailed information is given elsewhere [1,20].

2.2. Specimen preparation

2.2.1. Synthesis of nanotubes

Prefabricated oxCNTs and sol-gel method were used to achieve coatCNTs. Previous dispersion and ultra-sonication of the oxCNTs in ethanol introduces ester bonds on the surface of the oxCNTs as well as water in the system. The ester bonds enable the covalent coupling of molecules while the water in the system facilitates the hydrolysis of TEOS. Immediately upon addition of TEOS and ammonia as the basic catalyst into the solution, hydrolysis and nucleation of the TEOS occurred on the surface of oxCNTs. After adding, the mixture was 20 h stirred at 25°C, finally centrifuged and recovered particles dried 24 h at 100°C. Comparing with oxCNTs the formed silica layer can be seen (Fig. 1). Measured by simultaneous thermal analysis (STA), oxCNTs were stable up to ~515°C until a plateau was reached at ~740°C. This degradation (oxidation of CNTs) lead to a weight loss of 95.3% w/w and a residue of 4.7% w/w. Compared to coatCNTs degradation temperature was extended up to ~625°C and a weight loss of at most 10.0% w/w with at least 87.6% w/w residue.

To produce TiNTs modified hydrothermal synthesis was used [51]. Hereby, amorphous anatase was added in a teflon piston with 10M sodium hydroxide under reflux. The mixture was stirred at 110–150°C for 48 h. Afterwards, 0.1M HCl was added and washed or neutralized with water, respectively. Finally, calcination at 200°C occurred. The obtained TiNTs are shown in Fig. 1.

2.2.2. Preparation of nanoreinforced three-phase-foams

Dispersions containing 23% w/w NS were produced considering the minimum of zeta potential at pH 10 to receive the highest electrostatic repulsion of the particles and thus avoid agglomeration. Prior foaming the total betaine concentration in the dispersions was adjusted to 20 mmol/L which results in the most stable three-phase-foam (see 3.1 Study of foam stability). For comparison, the betaine concentration for all foams was kept equal. The homogenization and foaming were done using a continuous dynamic stirrer (Hobart). Foaming time was adjusted to 3.5 min. For nanoreinforcement, nanotube concentrations of 0.1, 0.3, 0.5, 0.8 and 1.0% w/w related to the amount of NS were added to the dispersion. Detailed information is given in Ref. [49].

2.2.3. Hardening of three-phase-foams

After preparation drying of the obtained foams takes place under normal conditions (23°C/50%rh/400–500 ppm CO_2) for 2 d. For the hardening process, dried three-phase-foams are stored in saturated $Ca(OH)_2$-solution. The foams are taken out of the solution after 7 d and stored on a plastic plate until complete drying.

3. Results

3.1. Study of foam stability

To adjust the content of surfactant, foam stability was measured at different betaine (B) concentrations. After foaming, densities were determined by filling wet-foams in beakers with defined volume and mass and taking the weight. After 10, 20, 30 and 60 min drained dispersion was decanted and loss of continuous phase calculated. It was shown that with a concentration of 20 mM B no loss of continuous phase can be observed after 60 min. Also, the resulting density of 62 kg/m^3 was the lowest at this concentration and thus the highest air entrainment reached. To provide comparability, same surfactant concentration of 20 mM B was used to prepare nanoreinforced three-phase-foams. The highest foam stabilities containing different nanotube contents were observed with 0.8% w/w oxCNTs, 0.5% w/w TiNTs and 1.0% w/w coatCNTs (Fig. 2). In case of coatCNTs no loss of continuous phase takes place. Compared to TiNT foams with a drain of ~20% w/w those with oxCNTs showed more drain of ~33% w/w up to 30 min. After 30 min no more loss of continuous phase proceeded.

All foams containing nanotubes show densities of 75–90 kg/m^3 and thus were denser compared to the reference foam (Table 2).

3.2. Study of microstructure

Immediately after foaming the pore size distributions of the most stable foams were determined by means of light microscopy (LM) and compared. Therefore, a MIA (multiple image arrangement) based on single microscopic images with an area of 13 mm^2 was captured after filling the wet foams in a transparent closed plastic container to get an even surface for detection. The pore shape was assumed as ideally circular and by manual measuring the pore area determined. With the help of the pore area, radii of the pores were calculated and by statistical frequency analysis the pore size distribution within the foam cross section was calculated. The pore radii of the reference were between 0.1 and 75 μm and foams with oxCNTs show radii of 2–74 μm. Foams with coatCNTs or TiNTs had larger pores of 3–85 or 3–88 μm, respectively. For all

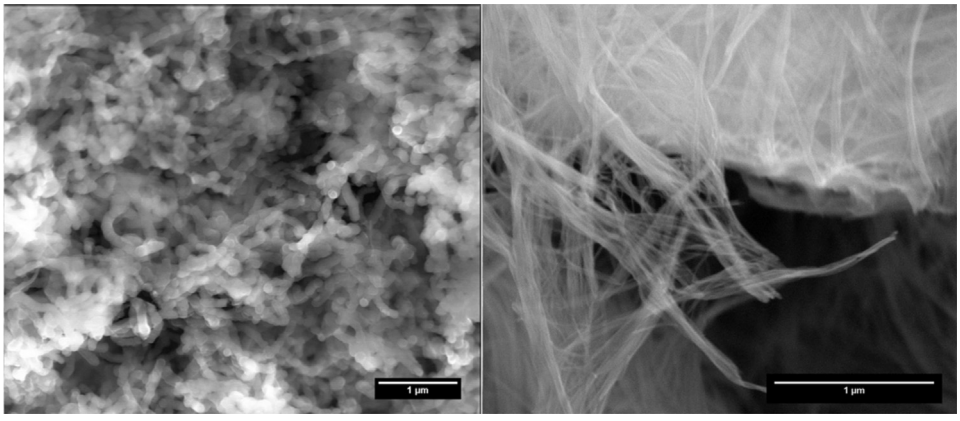

Fig. 1. SEM images of coated CNTs (left) and synthesized TiNTs; scale bar: 1 μm.

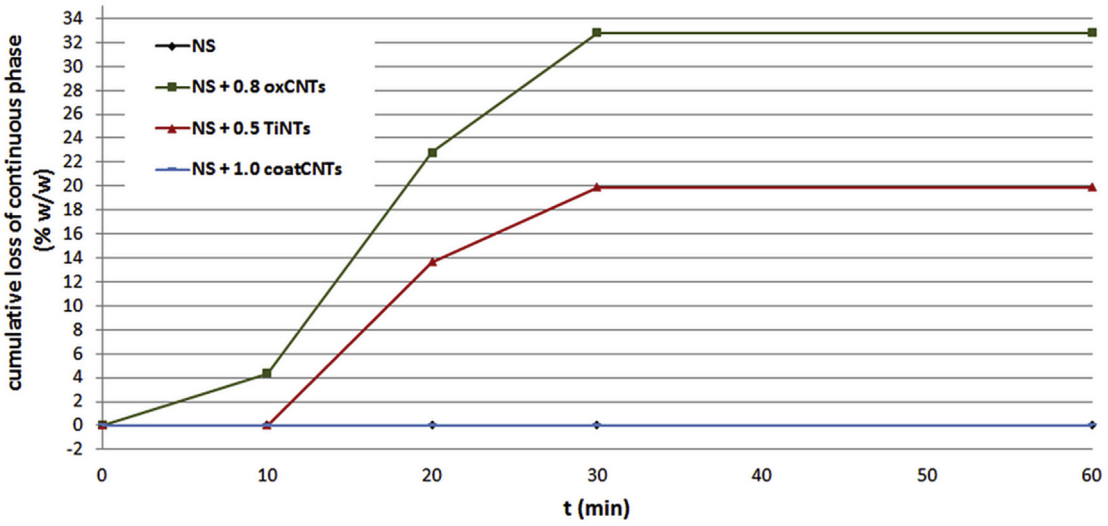

Fig. 2. Cumulative loss of continuous phase over time of the most stable nanoreinforced three-phase-foams.

Table 2
Densities of the most stable nanoreinforced three-phase-foams.

Samples	% w/w[a]	p (kg/m^3)
NS	–	62
NS+oxCNTs	0.8	80
NS+coatCNTs	1.0	90
NS+TiNTs	0.5	75

[a] Related to solid content of dispersion.

foams, ~90% of the detected pore radii were up to 30 μm (Fig. 3).

Additionally, pore radii were determined after storing in the closed container for 60 min so that no water diffusion can take place. Both foams with CNTs showed the largest pores of 200 μm. Compared to these foams with TiNTs and the reference had their maximum at 150 μm.

By LM and SEM, foam structures related to lamellae and the border widths as well as the structural density were estimated (Fig. 4). For the sample preparation, no sputtering was used. Reference foams and these with oxCNTs had a similar bone-like structure with conformal border widths and less destabilizing effects which were frozen after complete drying. Foams without tubes showed border widths of 50–100 μm and with oxCNTs 50–150 μm and both lamellae widths up to 1 μm (Table 3). For reinforced foams with coatCNTs larger border widths of 100–250 μm and thus a more inhomogeneous distribution of those can be observed. Lamellae widths were found as 1.0–1.5 μm. Border widths of TiNT foams were also 100–250 μm and lamellae widths between 0.5 and 1.5 μm. In addition, compared to the latter broader value of lamellae widths, these foams showed a high inhomogeneity related to the pore size distribution.

After hardening the porosity inside the borders was reduced.

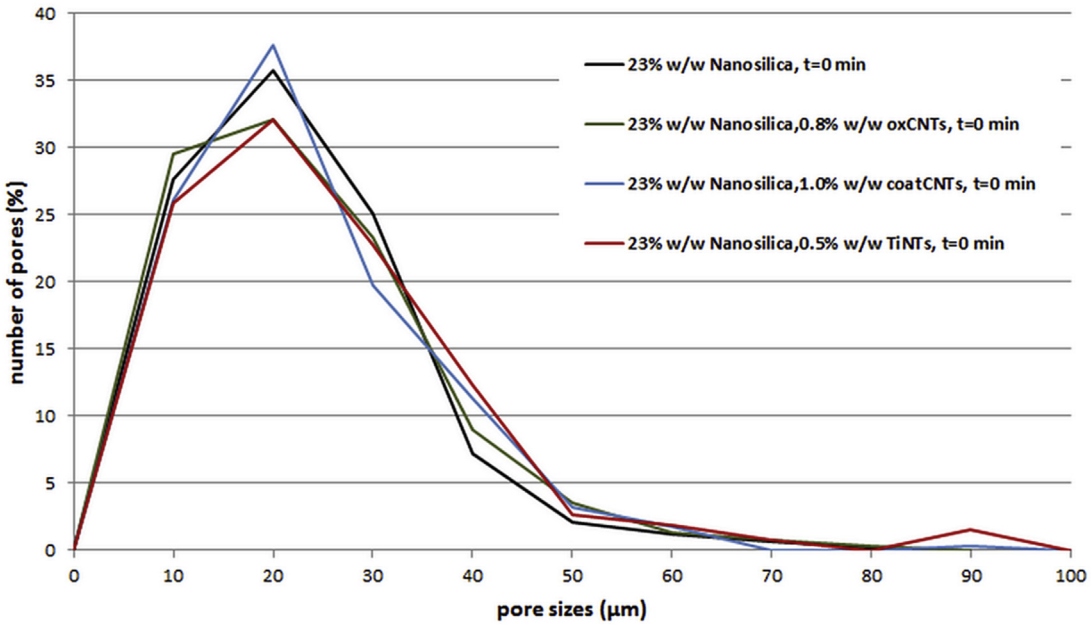

Fig. 3. Pore size distribution of the different most stable nanoreinforced three-phase-foams immediately after foaming (t = 0 min).

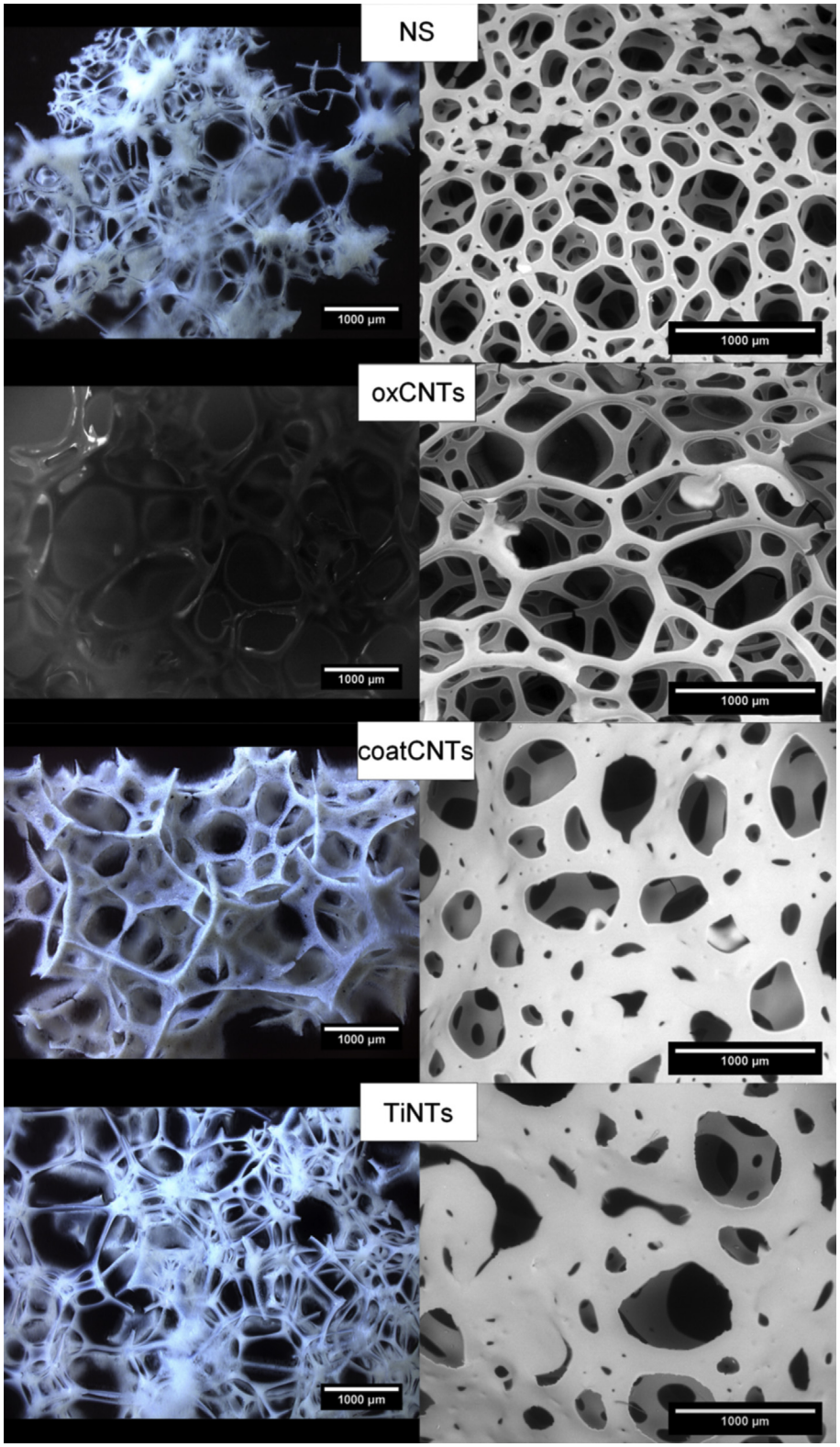

Fig. 4. LM and SEM investigations of nanoreinforced three-phase-foams before hardening and after dyring; scale bar: 1000 µm.

Border and lamellae widths were increased (Fig. 5). Reaction products like hexagonal shaped calcium hydroxide (CH) can be identified on the surface of the borders. Additionally, structures on the lamellae were built which could be assumed as C-S-H-phases (lower right).

Thus, microstructural investigations show that addition of nanotubes leads to differences in the foam structure. Three-phase-foams with oxCNTs were similar compared to these without nanotubes related to pore size distribution as well as border and lamellae widths. After hardening process oxCNTs show larger pore

Table 3
Influence of nanoreinforment and pozzolanic hardening on the border and lamellae widths as measured by SEM.

Samples	Border width (μm)	Lamellae width (μm)
NS	50–100	~1.0
NS_oxCNTs	50–150	0.5–1.0
NS_coatCNTs	100–250	1.0–1.5
NS_TiNTs	100–250	0.5–1.5
$NS_{hardened}$	50–150	1.0–1.5
$NS\_oxCNTs_{hardened}$	50–200	0.5–1.5
$NS\_coatCNTs_{hardened}$	100–300	1.5–2.5
$NS\_TiNTs_{hardened}$	100–300	1.0–2.0

sizes and thinner border widths compared to the reference. Foam stability with oxCNTs was decreased which can be explained by the sorption of betaine molecules on oxCNTs needed for equal foam stability as in the reference system. Thus, it can also be assumed that the remained foam stability is based on sterical effects or properties of oxCNTs, respectively. Compared to this, foams reinforced with coatCNTs and TiNTs show a slightly broader pore size distribution but especially larger border/lamellae widths before and after hardening process. Foam stability was lowered by TiNTs but less than with oxCNTs. The reason can be that less surface area is provided in case of TiNTs also by taking used amount into account. CoatCNTs have no destabilizing effects which can be explained by lower amounts of tubes in total due to the high percentage of nanosilica coating (87.7% w/w), less surface area and thus less sorption of betaine molecules. Microstructural investigations with the help of LM and SEM have shown that due to the hardening process porosity inside the foam structure was reduced and border/lamellae widths were increased. Indications for C-S-H-phases/C-S-H-gel and formation of CH crystals after hardening were found by SEM.

3.3. Study of phase development

STA was chosen to prove C-S-H-phases and examine other reaction products like CH and calcium carbonate (Cc) formed after hardening process. Energy dispersive X-ray spectroscopy (EDX) was done to determine formed reaction products as well as to check calcium distribution in the foam structure with the help of element mapping. In addition, X-ray powder diffraction (XRD) was used to get information related to crystalline phases.

A thermogram was recorded in temperature range of 25°C–1000°C at a heating rate of 10 K/min. Endo- or exothermic processes were identified on basis of the simultaneously recorded DSC-signal. All hardened three-phase-foams showed deposal of physically and chemically bound water up to ~130°C. It follows that the samples after storage in calcium hydroxide solution also show water deposal of C-S-H-phases [52] and physically bound water especially on the nanotube surface. Loss of bounded water was 0.5–1.5% w/w with the highest loss in case of oxCNTs which were also used in the highest amount. Hardened foams with nanotubes had in every case higher water deposal compared to the reference. De-hydration of CH took place at 300–450°C and Cc at 600–700°C. In Ref. [52] temperature ranges are given by 425–550°C for de-hydration and 680–760°C for de-carbonation. Thus, temperature ranges were shifted to lower temperatures which can indicate smaller particle sizes and amorphization. Amounts of CH were 1.9–3.6% w/w whereby hardened foams with TiNTs had the highest amount. Cc contents were 0.7–1.2% w/w and also in TiNTs reinforced foams highest amounts were identified. Also, decomposition of the different nanotubes was detected and started at 750°C. The decomposition process of nanotubes resulted in inserted mass ±0.2% w/w. By EDX analysis it was observed that calcium was homogeneously distributed in the foam structure. Also, the point and area element mapping enabled the assignment to the formed

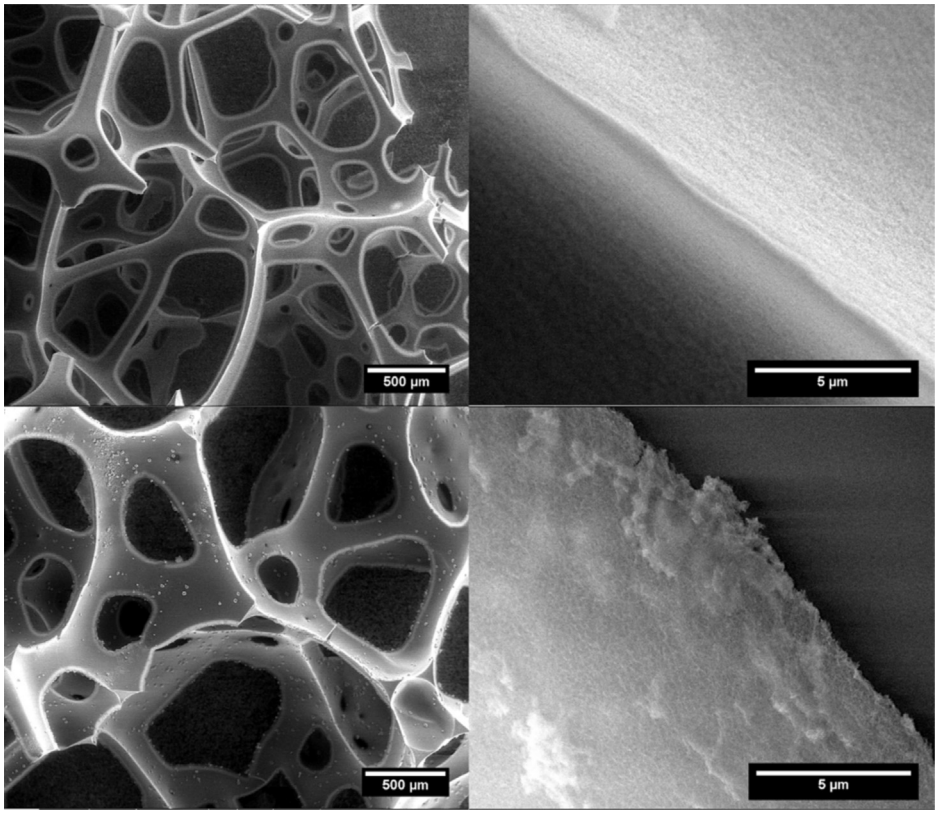

Fig. 5. SEM investigations of three-phase-foams before (upper left and right) and after hardening (lower left and right).

products. Calcium-to-silicon-ratios of the surface up to 0.1 and formed crystals up to 2.0 were calculated. With XRD formation of reaction products C-S-H and CH cannot be confirmed. However, all hardened foams – with and without nanotubes – showed crystalline Cc.

Thus, results of phase development confirm X-ray amorphous CH and C-S-H-phases through STA and EDX investigations. Also, Cc as the only crystalline product was determined with the help of XRD.

3.4. Pozzolanic reactivity

To examine the influence of the used additives on pozzolanic reactivity, a measurement series in saturated calcium hydroxide solution in presence of used NS particles was done. Therefore, saturated calcium hydroxide solution was prepared and appropriated amounts of the different additives were added. After adding, pH measurements were started and progressed up to 24 h. Solutions were ultra-filtered and calcium concentration as well as conductivity of the filtrate determined. Obtained filter cakes were dried at 35°C and further investigations of resulting microstructure and phase development were carried out.

For the measurements quantity of each additive was kept equal. Amount of NS were 0.125% w/w related to the used 200 g calcium hydroxide solution. Content of coatCNTs was dependent on the target to reach also 0.125% w/w NS by coating (0.285 g). TiNTs and oxCNTs amounts were calculated with the help of determined BET-surfaces to provide the same area (260 m^2) for sorption processes and further precipitation, for example. In every case the betaine concentration was set to 20 mM as in the foam preparation.

Results showed that the lowest pH, calcium concentration and conductivity were reached by using TiNTs with and without betaine (Table 4). Thus, it follows that TiNTs have a high Ca^{2+} affinity which adsorb on the surface and can also intercalate. Almost all samples show lower calcium concentration after 24 h with B due to chelating of Ca^{2+} through betaine molecules. Also, the highest conductivity with betaine content was measured for those which could be explained by the electrolyte sodium chloride in surfactant solution.

In case of oxCNTs, calcium concentration with surfactant is higher than without B and thus the adsorption of betaine molecules on the CNT surface could be preferred compared to Ca^{2+} ions. On the other hand, calcium ion concentration could be higher due to the additional sorption of surfactant molecules on NS surface whereby less B is available to chelate Ca^{2+} ions.

Comparing pH values of the solutions immediately after adding used additives, the tendency was similar to these of determined calcium concentration. Every sample excluding oxCNTs, showed the lowest pH with betaine and TiNTs. Finally, after 24 h solutions with TiNTs and oxCNTs without betaine had the lowest and NS or NS with betaine the highest pH, respectively. This could be explained due to the high surface area of nanotubes which can adsorb more calcium ions and act as heterogeneous seeds for the formation of calcium containing reaction products like C-S-H-phases, CH and Cc.

Table 4
Measurements of pH, concentration of calcium ions in solution (t = 24 h) and conductivity of saturated calcium hydroxide solution containing used additives.

Sample	Ca Conc. (ppm)	Conductivity (mS/cm)	ΔpH
NS	657.8	6.2	0.9
NS+B	522.2	8.6	0.4
NS+TiNTs	99.3	4.6	0.6
NS+TiNTs+B	85.8	5.8	0.6
NS+oxCNTs	281.7	3.7	0.5
NS+oxCNTs+B	450.6	7.1	0.5
coatCNTs	454.0	5.3	0.3
coatCNTs+B	431.0	7.4	0.6

The provided filter cakes were further investigated and compared by SEM with regard to formed reaction products. For sample preparation no sputtering was used. By comparing the different samples it can be concluded that in every case bigger crystals of CH were built without betaine (Fig. 6). Especially, coatCNTs showed crystals $\geq$2 μm. In every case betaine was added, very small crystals of CH can be observed. Also, except for oxCNTs with and without surfactant each sample provided C-S-H gel on the surface. In addition, samples with TiNTs were mainly covered with reaction products in both cases which explain low calcium concentrations in the filtrated solution.

With the help of STA measurements a semi-quantitative analysis of the filter cake was done to determine the formed reaction products after 24 h in saturated calcium hydroxide solution. Measurement settings were kept equal to those of three-phase-foams with and without nanotubes.

Each sample except oxCNTs with betaine showed water deposal above 100°C and up to 160°C with only NS added as a maximum. Thus, in these samples the water deposal in a broad range of 100–200°C indicates the formation of C-S-H-phases [52]. Related to the loss of physically and chemically bound water above 100°C and based on the assumption that this loss belongs to C-S-H dehydration, samples containing TiNTs had the highest C-S-H content. These were followed by NS and both coatCNTs samples. Lowest contents were reached through adding B to NS and by oxCNTs. Thus, B reduces or inhibits pozzolanic reaction. The missing loss of chemically bound water in case of oxCNTs lead to the conclusion that the adsorption of B molecules on the CNT surface inhibit the seeding effect which normally lead to an increased formation of calcium containing reaction products. Samples with B showed mass loss in a temperature range of 200–360°C and can be referred to formed hydrotalcite-like structures which show endothermic process at 285–440°C in Ref. [52]. Comparing the sum of CH and Cc, the samples with B showed the highest content but also coatCNTs samples were high in especially CH contents. Abbreviations of the different DSC signals resulted in peak shoulders of dehydration or de-carbonation, respectively, regarding NS and coatCNTs without betaine. This leads to the assumption that two different particle sizes were built whereas the smaller particles dehydrated or de-carbonated first. In addition, temperature ranges were shifted to lower ones compared to the literature [52] which also confirms not only smaller particle sizes but also could indicate amorphous structures. The formation of C-S-H-phases can also be confirmed due to an exothermic DSC signal without mass loss in TG signal and could be identified as re-crystallization from C-S-H (I) [52]. Finally, it should be taken into account that the de-hydration could not exactly be referred to only $Ca(OH)_2$, also a further later de-hydration of hydrotalcite-structure or semi decomposition of nanotubes are possible.

XRD measurements were carried out to determine the influence of the different additives with respect to formed crystalline phases. Patterns of NS showed mainly reflexes of Cc and a broad peak of X-ray amorphous SiO_2 (Fig. 7). In addition, sample with only NS shows less intensity of X-ray amorphous content of SiO_2 and thus could indicate pozzolanic reaction to C-S-H-phases. Also, reflexes related to C-S-H can be observed. Compared to this, NS+B showed broader peaks in case of calcite which could be explained by less crystallinity and smaller particle sizes. This trend was also observed for samples containing oxCNTs and TiNTs. CoatCNTs without B was the only sample showing indications for crystalline CH at 18.5 2-Theta (Fig. 8). Thus, CH observed in STA is mainly X-ray amorphous.

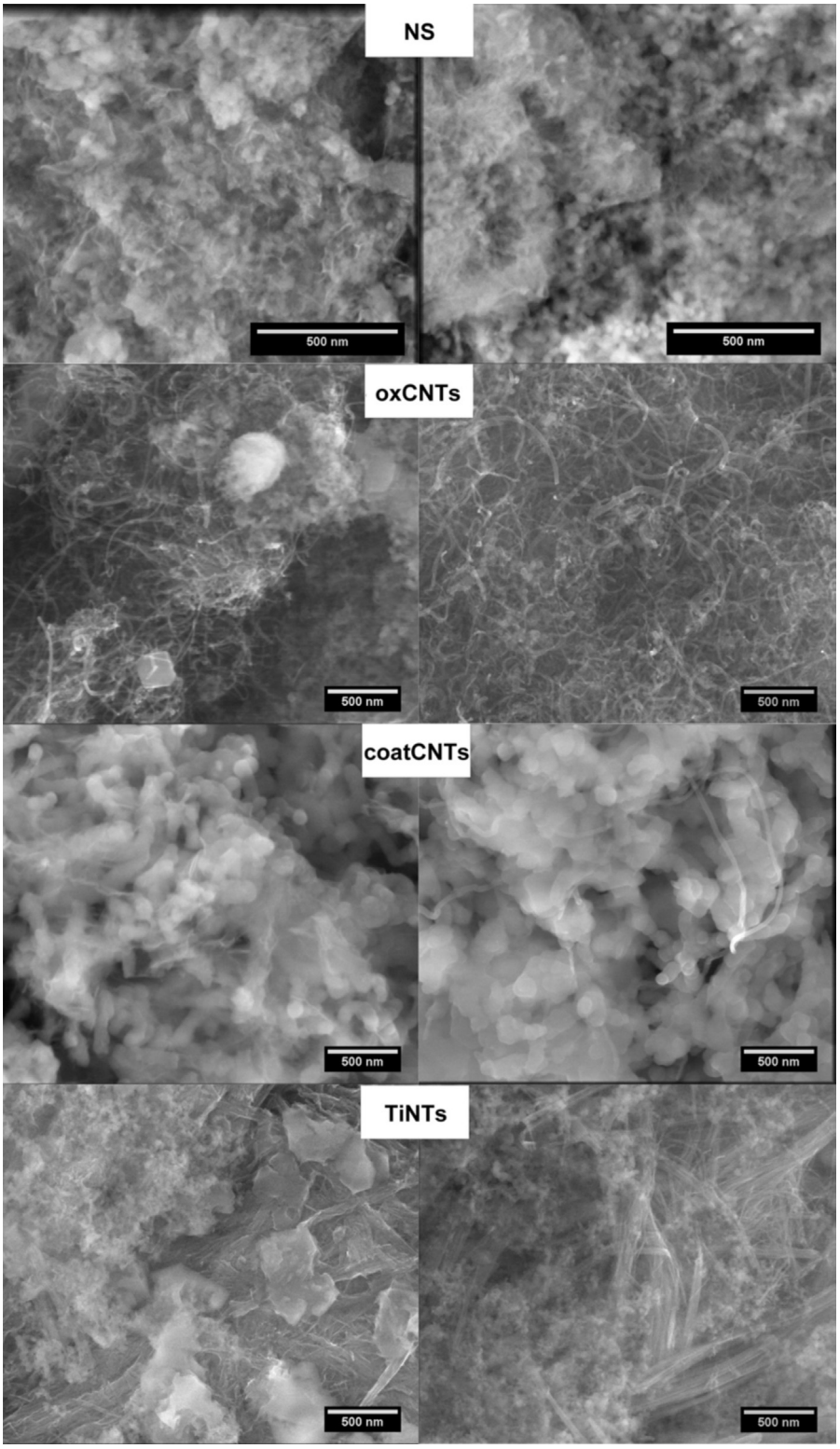

Fig. 6. SEM images of the resulting reaction products after pozzolanic reaction (t = 24 h) influenced by the different used additives without (left) and with B (right); scale bar: 500 nm.

In case of coatCNTs with B only low intensities of calcite reflexes and one reflex below 10 2-Theta can be seen which could be referred to hydrotalcite-like structures (Fig. 8). Due to this and previous STA results, the assumption was made that B also forms further reaction products with calcium hydroxide in solution. After adding B in saturated calcium hydroxide solution, precipitation takes place. The product was filtered and investigated by XRD. The resulting pattern showed the expected hydrotalcite-like structure which can also be found in the sample of coatCNTs with B. More investigations of this precipitate or reaction product, respectively,

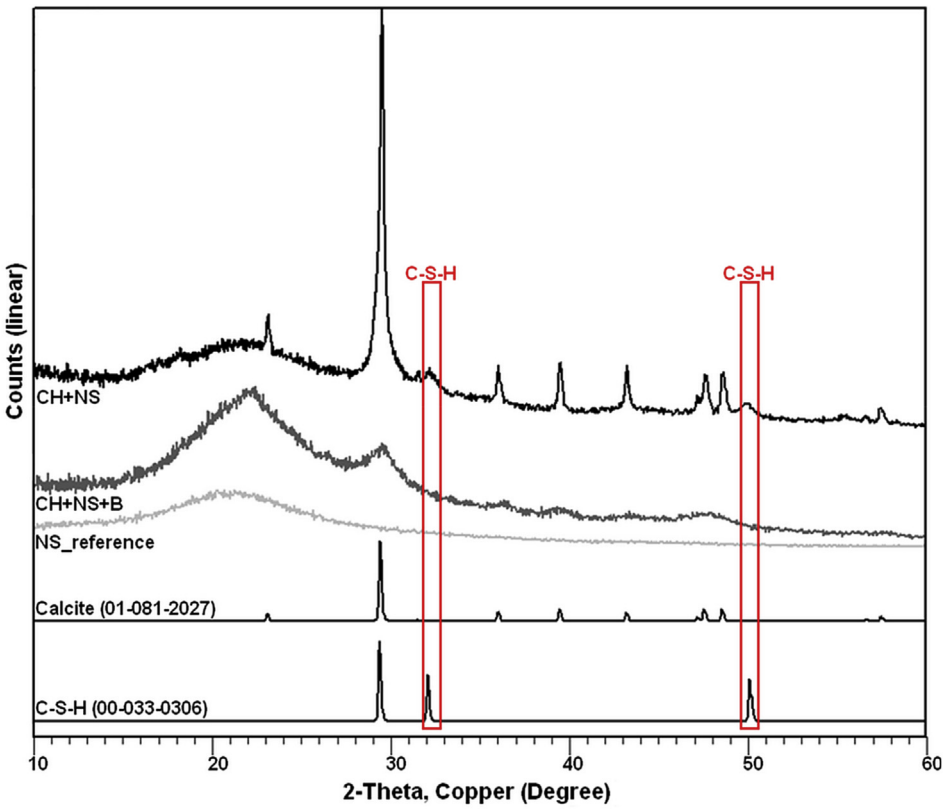

Fig. 7. XRD patterns of samples NS and NS+B compared to reference patterns.

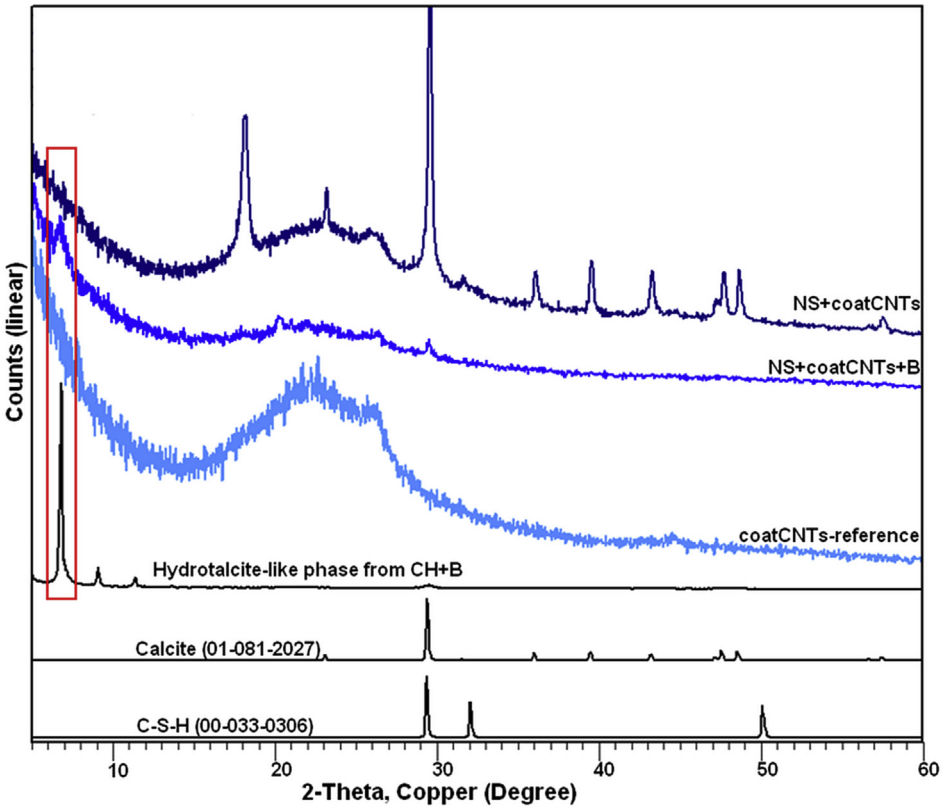

Fig. 8. XRD patterns of samples NS+coatCNTs and NS+coatCNTs+B compared to CH+B and reference patterns.

will be published in more detail in further research.

To summarize, investigations on the pozzolanic reactivity show first insights in the interaction of used nanomaterials and surfactant with Ca^{2+} ions. Samples with TiNTs had the lowest calcium concentration due to high Ca^{2+} affinity. Almost all samples with betaine had the lowest calcium concentration and highest conductivity caused by chelating of calcium ions through betaine molecules and the electrolyte sodium chloride in used betaine solution. Filtrate of oxCNTs with B showed higher calcium amount which leads to the assumption that betaine molecules are preferred to adsorb on oxCNT or additional sorption on NS which leads to less chelating. These observations can also be confirmed by pH measurements at the beginning. After 24 h, samples with TiNTs and oxCNTs without betaine provide the lowest and NS with and without B the highest pH. It follows that this is affected by high surface area of nanotubes which offers more sorption ability and seeding for the formation of reaction products.

With the help of SEM C-S-H gel was observed for each sample without B and excluding oxCNTs with and without B. Every sample showed smaller CH crystals with betaine and samples containing TiNTs were mainly covered by reaction products.

By STA it was figured out that beside oxCNTs with B every sample show water deposal above 100°C up to 160°C which indicates C-S-H-phases. This was also confirmed by re-crystallization process from C-S-H at higher temperatures. In every case by adding betaine de-hydration temperature ranges related to hydrotalcite-like phases can be assumed. In addition, temperatures ranges of de-hydration and de-carbonation were shifted to lower temperatures and peak shoulders in DSC signals observed could be explained by different crystal sizes or formation of amorphous products, respectively.

With the help of XRD measurements indication of different particle sizes results due to broader peak of calcite, for example. This indicates not only smaller particle sizes but also less crystallinity, especially in presence of B. Thus, these two properties are assumed to be mainly determined by sorption of B molecules on specific crystal planes. Also, reflexes of C-S-H-phases can be found for NS and thus results of SEM and STA can be confirmed. The only sample which show reflexes for crystalline CH is coatCNTs without B. Thus, CH found in STA is mainly X-ray amorphous for all samples. In addition, hydrotalcite-like structures observed in STA and XRD were formed by B in calcium hydroxide solution.

4. Conclusions

Finally, different properties of three-phase-foams were figured out by using several types of nanotubes. After drying, the foams show no more destabilizing influences. The most stable wet three-phase-foams were prepared without nanotubes and with coatCNTs. All in all, stability of the resulting foams is also related to betaine adjustment which has to be done in further investigations. The pore size distribution was shifted to smaller pore sizes compared to previous investigation due to improved foaming conditions. Due to hardening process porosity in the foam structures was reduced, lamellae/border widths increased and strengthening reaction products like C-S-H-phases or Cc were built, respectively.

Investigating influences of used additives on pozzolanic reactivity lead to the conclusion that C-S-H-phases were formed in almost every sample but are strongly influenced by the surfactant betaine. The latter also results in the formation of hydrotalcite-like structures in calcium hydroxide solution. Also, betaine has a big influence on the crystallinity and particle sizes of both calcium hydroxide and carbonate. In addition, it was shown that TiNTs have a high calcium affinity but oxCNTs tend to adsorb preferred betaine molecules. Thus, the formation of reaction products and foam stability is mainly referred to the used surfactant which provides a high sorption ability.

In sum, a waiver of thermal treatment or additional binders should be possible as well as produce future lightweight materials with densities of less than 100 kg/m^3 and based on long-chain environmentally friendly surfactant. These advantages lead to energy and cost savings in the production of raw materials. Moreover, well-dispersed nanotubes in three-phase-foams could further integrate in other binding materials to adapt certain properties of those and also provide strengthening reaction products by seeding effect or pozzolanic reaction, respectively.

Acknowledgment

The authors express their thanks to the workers of the institute of building materials chemistry at the University of Siegen, especially to T. Müller, Dr. C. Pritzel and Dr. Y. Sakalli for their support.

References

[1] C. Krämer, M. Schauerte, T.L. Kowald, R.H.F. Trettin, Three-phase-foams for foam concrete application, Mater. Charact. 102 (2015) 173–179.
[2] M. Scheffler, P. Colombo, Cellular Ceramics. Structure, Manufacturing, Properties and Applications, Wiley-VCH, Weinheim, 2005.
[3] R. Lakes, Materials with structural hierarchy, Nat. [Online] 361 (6412) (1993) 511–515.
[4] J.J. Bikerman, Foams, Springer-Verlag, New York, 1973.
[5] A.J. Wilson (Ed.), Foams: Physics, Chemistry and Structure, Springer Series in Applied Biology, London, 1989.
[6] R.K. Prud'homme, S.A. Khan, Foams. Theory, Measurements and Applications, CRC Press, New York, 1996.
[7] D.L. Weaire, S. Hutzler, The Physics of Foams, Clarendon Press, Oxford, 1999.
[8] E. Dickinson, Adsorbed protein layers at fluid interfaces: interactions, structure and surface rheology, Colloids Surf. B Biointerfaces 15 (2) (1999) 161–176.
[9] P.J. Wilde, Interfaces: their role in foam and emulsion behaviour, Curr. Opin. Colloid Interface Sci. 5 (3–4) (2000) 176–181.
[10] K. Holmberg, Handbook of Applied Surface and Colloid Chemistry, John Wiley&Sons, Chichester, 2002.
[11] S.U. Pickering, Emulsions, J. Chem. Soc. 91 (1907) 2001–2021.
[12] V.B. Menon, D.T. Wasan, Particle-Fluid interactions with application to solid-stabilized emulsions, Part I: the effect of asphaltene adsorption, Colloids Surf. 19 (1986) 89–105.
[13] B.P. Binks, Particles as surfactants-similarities and differences, Curr. Opin. Colloid Interface Sci. 7 (1–2) (2002) 21–41.
[14] Z. Du, M.P. Bilbao-Montoya, B.P. Binks, E. Dickinson, R. Ettelaie, B.S. Murray, Outstanding stability of particle-stabilized bubbles, Langmuir 19 (8) (2003) 3106–3108.
[15] E. Dickinson, R. Ettelaie, T. Kostakis, B.S. Murray, Factors controlling the formation and stability of air bubbles stabilized by partially hydrophobic silica nanoparticles, Langmuir 20 (20) (2004) 8517–8525.
[16] B.P. Binks, T.S. Horozov, Aqueous foams stabilized solely by silica nanoparticles, Angew. Chem. Int. Ed. [Online] 44 (24) (2005) 3722–3725.
[17] P. Stevenson, Foam Engineering. Fundamentals and Applications, second ed., John Wiley & Sons, Hoboken, 2012.
[18] U.T. Gonzenbach, A.R. Studart, E. Tervoort, L.J. Gauckler, Ultrastable particle-stabilized foams, Angew. Chem. Int. Ed. 45 (21) (2006) 3526–3530.
[19] A.R. Studart, U.T. Gonzenbach, E. Tervoort, L.J. Gauckler, Processing routes to macroporous ceramics: a review, J. Am. Ceram. Soc. 89 (6) (2006) 1771–1789.
[20] C. Krämer, T.L. Kowald, R.H.F. Trettin, Pozzolanic hardened three-phase-foams, Cem. Concr. Compos 62 (2015) 44–51.
[21] L.V. Radushkevich, V.M. Lukyanovich, O strukture ugleroda, obrazujucegosja pri termiceskom razlozenii okisi ugleroda na zeleznom kontakte, Zurn Fis. Chim. 26 (1952) 88–95.
[22] S. Iijima, Helical microtubules of graphitic carbon, Nature 354 (6348) (1991) 56–58.
[23] S. Sinha, S. Barjami, G. Iannacchione, et al., Off-axis thermal properties of carbon nanotube films, J. Nanopart. Res. 7 (6) (2005) 651–657.
[24] E.T. Thostenson, L. Chunyi, T.-W. Chou, Nanocomposites in context, Compos. Sci. Technol. 65 (3–4) (2005) 491–516.
[25] B. Demczyk, Y. Wang, J. Cumings, et al., Direct mechanical measurement of the tensile strength and elastic modulus of multiwalled carbon nanotubes, Mater. Sci. Eng. A 334 (1–2) (2002) 173–178.
[26] M. Yu, Strength and breaking mechanism of multiwalled carbon nanotubes under tensile load, Science 287 (5453) (2000) 637–640.
[27] T. Guo, P. Nikolaev, A.G. Rinzler, et al., Self-assembly of tubular fullerenes, J. Phys. Chem. 99 (27) (1995) 10694–10697.
[28] M. Bierdel, S. Buchholz, V. Michele, et al., Industrial production of multiwalled carbon nanotubes, Phys. Status Solidi (b) 244 (11) (2007) 3939–3943.

[29] T. Seeger, T. Köhler, T. Frauenheim, et al., Nanotube composites: novel SiO2 coated carbon nanotubes, Chem. Commun. 1 (2002) 34–35.
[30] Q. Fu, C. Lu, J. Liu, Selective coating of single wall carbon nanotubes with thin SiO2 layer, Nano Lett. 2 (4) (2002) 329–332.
[31] H. Li, C.-S. Ha, I. Kim, Fabrication of carbon nanotube/sio(2) and carbon nanotube/sio2/Ag nanoparticles hybrids by using plasma treatment, Nanoscale Res. Lett. 4 (11) (2009) 1384–1388.
[32] M. Zhang, Y. Wu, X. Feng, et al., Fabrication of mesoporous silica-coated CNTs and application in size-selective protein separation, J. Mat. Chem. 20 (28) (2010) 5835.
[33] V. Butters, T. Kowald, M. Mahjoori, R. Trettin, Surface modified Carbon Nanotubes for an enhanced interaction with cement based binders, in: Nanotechnology in Construction – Proceedings of NICOM5, Springer international Publishing, 2015, pp. 253–258.
[34] G. Du, Q. Chen, R. Che, Z. Yuan, L. Peng, Preparation and structure analysis of titanium oxide nanotubes, Appl. Phys. Lett. 79 (22) (2001) 3702–3704.
[35] Y. Suzuki, S. Yoshikawa, Synthesis and thermal analyses of TiO2-derived nanotubes prepared by the hydrothermal method, J. Mater. Res. 19 (4) (2004) 982–985.
[36] D.V. Bavykin, J.M. Friedrich, A.A. Lapkin, F.C. Walsh, Stability of aqueous suspensions of titanate nanotubes, Chem. Mater 18 (2006) 1124–1129.
[37] T. Kasuga, M. Hiramatsu, A. Hoson, T. Sekino, K. Niihara, formation of titanium oxide nanotube, Langmuir (1998) 3160–3163.
[38] Yao B., Chan Y., Zhang X., Zhang W., Yang Z., Wang N. Formation mechanism of TiO2 nanotubes. Appl. Phys. Lett. 82:281–283.
[39] W. Wang, O.K. Varghese, M. Paulose, C.A. Grimes, Q. Wang, E.C. Dickey, A study on the growth and structure of titania nanotubes, J. Mater. Res. 19 (2) (2004) 417–422.
[40] Q. Chen, G. Du, S. Zhang, L. Peng, The structure of trititanate nanotubes, Acta Crystallogr. B (2002) 587–593.
[41] L. Pavlová, K. Slouf, Preparation and structure of TiO2 nanotubes, Mat. Struct. 13 (3) (2006) 156–157.
[42] J. Yang, Z. Jin, X. Wang, W. Li, J. Zhang, S. Zhang, X. Guo, Z. Zhang, Study on composition, structure and formation process of nanotube $Na_2Ti_2O_4(OH)_2$, Dalton Trans. (2003) 3898–3901.
[43] J.E. Boercker, E. Enache-Pommer, E.S. Aydil, Growth mechanism of titanium dioxide nanowires for dye-sensitized solar cells, Nanotechnology 19 (2008) 2008.
[44] C.-C. Tsai, H. Teng, Structural features of nanotubes synthesized from NaOH treatment on TiO_2 with different post-treatments, Chem. Mat. 18 (2) (2006) 367–373.
[45] P. Hoyer, formation of a titanium dioxide nanotube array, Langmuir (1996) 1411–1413.
[46] D. Gong, C.A. Grimes, O.K. Varghese, W. Hu, R.S. Singh, Z. Chen, E.C. Dickey, Titanium oxide nanotube arrays prepared by anodic oxidation, J. Mater. Res. 16 (12) (2001) 3331–3334.
[47] D.V. Bavykin, B. Cressey, F.C. Walsh, Low-temperature synthesis of titanate nanotubes in aqueous KOH, Austr. J. Chem. 60 (2) (2007) 95–98.
[48] K.G. Böttger, J. Thieme, R. Trettin, A. Korpa, C. Schmidt, Pozzolanic reactivity of nanoscale pyrogene oxides and their strength contribution in cement-based systems, Adv. Cem. Res. 20 (1) (2008) 35–46.
[49] C. Krämer, T. Kowald, V. Butters, R.H.F. Trettin, Carbon nanotube-stabilized three-phase-foams, J. Mater. Sci. 51 (8) (2016) 3715–3723.
[50] C. Krämer, T. Kowald, R. Trettin, Three-phase-foams as new lightweight materials and their use in foam concretes, in: Nanotechnology in Construction – Proceedings of NICOM5, Springer International Publishing, 2015, pp. 435–439.
[51] M. Ali, C. Pritzel and R. Trettin, Synthesis of titania nanoparticles and study of its influence in cementitious systems, In: *Nanotechnology in Construction – Proceedings of NICOM5*, 2015
[52] S.M. Kim, Y. Jun, C. Lee, J.E. Oh, Use of CaO as an activator for producing a price-competitive non-cement structural binder using ground granulated blast furnace slag, Cem. Conr. Res. 54 (2013) 208–214.
[53] C. Krämer, M. Schauerte, T. Kowald, R. Trettin, CNT-stabilized foam concrete on the basis of ultrahigh performance concrete (UHPC), in: 14th International Congress on the Chemistry of Cement, Abstract Book II, 2015, p. 377.
[54] C. Krämer, Z. Dang, R. Trettin, UHPC foam concretes on the basis of three-phase-foams, in: 4th International Symposium on Ultra-High Performance Concrete and High Performance Construction Materials, Conference Proceedings, vol. 27, 2016, pp. 15–16.

List of abbreviations

B: betaine
NS: nanosilica
CH: calcium hydroxide
Cc: calcium carbonate
TiNTs: titanate nanotubes
oxCNTs: oxidized carbon nanotubes
coatCNTs: coated carbon nanotubes
TEOS: tetraethyl orthosilicate
C-S-H: calcium-silicate-hydrate
CVD: chemical vapor deposition
CCVD: catalytic chemical vapor deposition
BET: Brunauer-Emmert-Teller
EDX: energy dispersive X-ray spectroscopy
LM: light microscopy
MIA: multiple image arrangement
SEM: scanning electron microscopy
STA: simultaneous thermal analysis
XRD: X-ray powder diffraction
IUPAC: International Union of Pure and Applied Chemistry